Geochemical Journal, Vol. 40, pp. 277 to 290, 2006

Evidence of primitive melt heterogeneities preserved in plagioclase-hosted melt inclusions of South Atlantic MORB

MARCO MAGNANI,[1]* TOSHITSUGU FUJII,[1] YUJI ORIHASHI,[1] ATSUSHI YASUDA,[1] TAKAFUMI HIRATA,[2] ALBA P. SANTO[3] and GLORIA VAGGELLI[4]

[1]Earthquake Research Institute, The University of Tokyo, Bunkyo-ku, Tokyo 113-0032, Japan
[2]Laboratory for Planetary Sciences, Tokyo Institute of Technology, 2-12-1 Ookayama, Meguro-ku, Tokyo 152-8550, Japan
[3]Dipartimento di Scienze della Terra via La Pira, 4 - 50121 Firenze, Italy
[4]CNR - Istituto di Geoscienze e Georisorse - Sezione di Torino c/o Dipartimento di Scienze Mineralogiche e Petrologiche Università di Torino Via Caluso, 35 I-10125 Torino, Italy

(*Received March 3, 2005; Accepted December 12, 2005*)

Melt inclusions contained in plagioclase and olivine phenocrysts have been studied in tholeiitic basalts from the Shona ridge-centered hot spot region, South Atlantic Ocean. Two types of primitive melt inclusions exist within a hand sample, Normal-Mid Ocean Ridge Basalt (N-MORB) and Enriched-Mid Ocean Ridge Basalt (E-MORB) as defined by trace elements. The N-MORB melt inclusions have low $(La/Sm)_n$ (0.54–0.72), high Zr/Nb (22–44) and depleted Light Rare Earth Element (LREE) patterns, whereas the E-MORB melt inclusions have high $(La/Sm)_n$ (0.79–1.09), low Zr/Nb (12–21) and flat LREE. The composition of melt inclusions has been modified by post-entrapment crystallization of the host phase, but this effect is considered relatively small and does not affect the incompatible trace element ratios. The matrix glasses have mildly E-MORB compositions that lie between the two different types of melt inclusions, suggesting that they are produced by mixing of primary magmas of E-MORB and N-MORB type.

The N-MORB primitive melt inclusions are geochemically similar to Indian and other South Atlantic N-MORB in having high Ba/Nb ratios (4–10), but for the first time much more extreme values are found (8–18). The reason for this anomalous enrichment can be related to the presence of old pelagic sediments in a regionally depleted asthenosphere.

The melt inclusions of this study display positive anomalies of Sr and Eu, the first time that have been recorded in the South Atlantic. Their characteristics could be explained by partial melting of mantle containing recycled oceanic crust.

Keywords: melt inclusions, plagioclase phenocrysts, South Atlantic, MORB, Shona

INTRODUCTION

The South Atlantic MORBs (40–55°S) are particularly complex from a geochemical point of view. Nevertheless the recent extensive studies of isotopes, major and trace elements on MORB glasses have helped to define regional geochemical domains in this region, distinguishing areas influenced by plumes (Shona and Discovery) from the areas where the MORB source is represented by a depleted asthenospheric mantle (Le Roux *et al*., 2002a; Andres *et al*., 2002; Douglass *et al*., 1999; Sarda *et al*., 2000).

From these studies it is evident that the Indian and South Atlantic shallow mantle has been contaminated by an old crustal component (oceanic crust + pelagic sediments) (Le Roux *et al*., 2002a; Rehkamper and Hofmann, 1997), but in the Shona region there is a lack of highly enriched MORB and the hot spot end-member is still unknown, on the basis of bulk rocks and glass compositions (Le Roux *et al*., 2002a). Melt inclusions studies have not been done in the Shona hot spot region, but the unique occurrence, reported in this study, of two tholeiitic samples bearing a huge number of primitive melt inclusions (Mg value = 0.67–0.70), trapped in high An plagioclase phenocrysts, exceptionally gave us the opportunity to study MORB samples with the aim of distinguishing the source end members and to obtain information on the magmatic evolution processes.

The ridge basalts were not considered to have a great compositional variation, notwithstanding in the last two decades the study of melt inclusions has proved that the magmas have a huge variability, particularly in trace elements, even at a small scale (Sobolev and Shimizu, 1993; Nielsen, 1995). The systematic of this variability is still under discussion, and one of the main arguments is the coexistence of E-MORB and N-MORB melts in the same specimen or even the same crystal (Slater *et al*., 2001). We could divide the models in two main streams, one

*Corresponding author (e-mail: Marukoma@eri.u-tokyo.ac.jp)

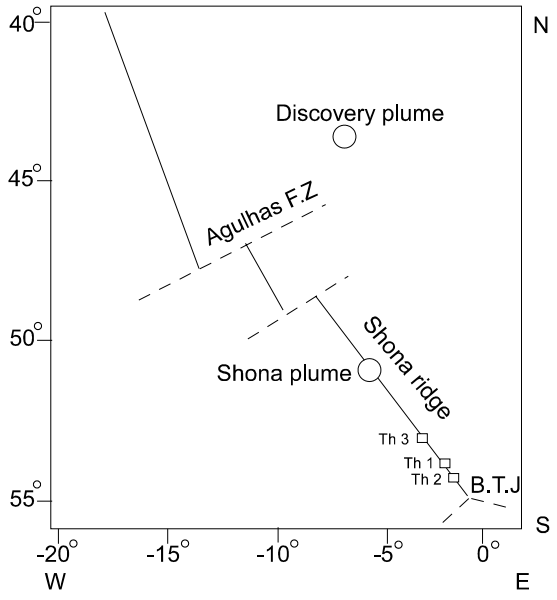

Fig. 1. Schematic map of the area of sampling in the South Atlantic Ocean. The Shona hot spot is considered to be on axis in proximity of the Bouvet triple junction (B.T.J) whereas Discovery plume is off axis northern from the Shona ridge. Th 1, th 2 and th 3 are the tholeiites object of this study.

supporting the origin of E-MORB and N-MORB as originated by the polybaric partial melting of an homogeneous source (Sobolev and Shimizu, 1993; Nielsen *et al*., 1995; Gurenko and Chaussidon, 1995; Mckenzie, 2000; Jull *et al*., 2002; Sims *et al*., 2002) and another one requiring the presence of a heterogeneous source (Sours-Page, 1999; Le Roux *et al*., 2002a). In the case of South Atlantic region an extensive database of both trace elements and isotopes is available, then by coupling these data with those from the melt inclusions of this study we attempt to explain the origin of E-MORB and N-MORB melts in the Shona Ridge.

All melt inclusions can be modified by post-entrapment crystallization of the host (e.g., Schiano 2003; Sinton *et al*., 1993) or by chemical diffusion through host minerals (e.g., Michael *et al*., 2002; Scowen *et al*., 1991, Cottrell *et al*., 2002) that could alter the original composition. We discuss the importance of these processes and show that the incompatible element ratios can be considered as accurately representing primary melts.

Samples and Petrographic Description

Three MORB samples S18-63-1, S18-62-2, G96-25-01 (renamed th 1, th 2 and th 3) were sampled during the 1994 (Strakhov) and 1996 (Gelendzihik) oceanic cruises (Carrara *et al*., 1997; Ligi *et al*., 1999, 1997) in a southern ridge segment of the South Atlantic Ocean, part of

Table 1. Analysis of tholeiitic bulk rocks

	th 1	th 2	th 3
SiO_2	47.2	48.2	47.3
TiO_2	1.07	1.97	1.04
Al_2O_3	22.6	15.9	17.9
Fe_2O_3	1.9	3.5	2.0
FeO	5.6	8.6	7.5
MnO	0.13	0.21	0.17
MgO	5.4	6.6	10.5
CaO	13.5	11.8	10.5
Na_2O	2.1	2.6	2.6
P_2O_5	0.11	0.20	0.11
K_2O	0.05	0.12	0.05
LOI	0.3	0.3	0.4

Unit: wt%.

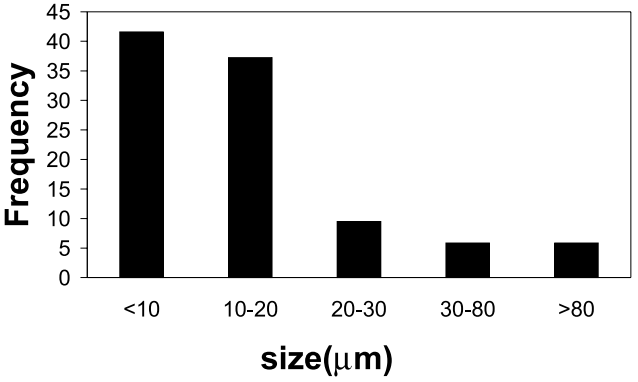

Fig. 2. Size frequency distribution of melt inclusions.

the ridge centered Shona hot spot area at 54°16′ S, 1°17′ W (th 1) 54°10′ S, 1°23′ W (th 2) and 53°28′ S, 3°2′ W (th 3) (Fig. 1). The specimens of th 1 and th 2 are highly phyric, containing large and abundant plagioclase phenocrysts together with rare (1–2%) olivine and spinel microphenocrysts, and have a mildly evolved glassy groundmass (Table 2). The specimen of th 3 is also highly phyric but is richer in olivine phenocrysts than plagioclases and is quite primitive (Table 1).

The plagioclase phenocrysts are generally very large (>1000 μm), having broad homogeneous cores (An 84–90%) and thin sodic rims (An 69–73.9%—Table 3). The melt inclusions trapped by the plagioclase phenocrysts are particularly abundant, even hundreds in the same phenocryst, commonly <30 μm in diameter (Fig. 2), and have a circular or ellipsoidal shape being arranged in bands or clusters, whereas the melt inclusions larger than 30 μm are distributed more randomly and are often elongated. Number and distribution of melt inclusions in plagioclase phenocrysts vary within different crystals, do

Table 2. Melt inclusions and matrix glasses analysis

	*G.M th 1	RSD (%) $n = 10$	*G.M th 2	RSD (%) $n = 10$	*M.I 1plg 1 th 1	RSD (%) $n = 5$	*M.I 2plg1 th 1	RSD (%) $n = 5$	**M.I 3plg1 th 1	RSD (%) $n = 5$	**M.I 4plg1 th 1	RSD (%) $n = 5$	***M.I 5plg1 th 1	RSD (%) $n = 5$	***M.I 10plg1 th 1	RSD (% $n = 5$
Major (wt%)																
SiO_2	50.80	0.55	49.84	0.63	50.50	0.49	49.90	0.48	50.26	0.51	50.08	0.53	50.14	0.85	50.55	0.77
TiO_2	1.80		2.15		0.84		1.10		0.97	13.62	0.99	8.31	0.96		0.93	1.28
Al_2O_3	14.30		14.60		14.00	0.63	14.10		14.14	0.65	14.28	0.62	14.28	0.43	14.18	0.42
FeO_{tot}	10.60		11.30		8.80		8.50	0.54	8.94	0.13	8.66	2.49	8.35		8.41	1.10
MnO	0.18	17	0.17	13	0.16	24	0.16	18	0.12	36.40	0.16	18.21	0.17		0.17	8.56
MgO	7.10		6.80		10.70		10.50		11.02	3.45	10.74	0.77	10.88		10.77	1.57
CaO	11.10		10.60		12.00		12.20		11.88	0.09	11.88	1.71	11.73		11.74	1.03
Na_2O	2.50		2.80		2.00		2.02		1.95	2.93	2.03	3.78	2.08		1.97	9.45
P_2O_5	0.30	13	0.33		0.33		0.30		0.29	2.19	0.31	8.49	0.18	12	0.14	6.79
K_2O	0.18		0.26	10	0.11		0.11		0.09	6.02	0.11	15.68	0.08	11	0.09	2.70
Mg value	0.54		0.51		0.69		0.69		0.67		0.69		0.70		0.70	
Total	99.40		99.20		99.68		99.14		99.97		99.52		98.92		99.02	
Trace (ppm)		$n = 10$		$n = 10$		$n = 5$		$n = 4$		$n = 3$		$n = 5$		$n = 3$		$n = 2$
Ba						11		11				18				20
Ce					5.14	10	4.42		6.28		6.31		7.89		7.25	19
Dy	5.30	11	6.00	15	2.89	20	2.19	19	3.43	16	3.22	24	3.18		2.90	16
Er	3.30	10	3.52	17	1.58	12	1.37		2.31	13	2.55	19	1.84		1.66	24
Eu	1.20	11	—	—	0.84	23	0.84	18	0.90	13	0.98	>30	0.89		0.94	19
Hf	b.d	b.d	b.d	b.d	1.4	24	0.92	>30	1.42	24	—	—	1.01		1.25	19
La	5.00		6.30		1.88	11	1.48		1.73		2.14		2.63		2.24	17
Nb	4.80		5.90		1.11		0.81		1.38		1.56	14	3.16		1.18	
Nd	9.80				4.84	15	4.20		6.07	16	6.59	23	5.61		6.47	19
Pb	—	—	—	—	—	—	—	—	0.41	27	—	—	0.38		0.41	14
Rb	2.89	>30	0.40	>30	0.64	>30	b.d	b.d	1.30	16	1.44		2.47	16	1.77	14
Sm	3.40	13	4.50	10	1.86	28	1.41	24	2.00		2.29	27	1.91	28	2.15	
Sr	107		113						104						105	
Ta	0.20	19	0.30	>30	0.09	>30	0.04	>30	0.09	10	—	—	0.17		0.08	>30
Th	0.40	28	0.50	27	0.19	>30	0.03	>30	0.09	>30	—	—	0.18	14	0.09	24
U	0.08	>30	0.14	>30	0.16	>30	0.09	>30	0.03	>30	—	—	0.08	>30	0.03	>30
Y				10												10
Yb	2.90	10	3.70	28	1.50	12	1.21	14	2.10		1.62	>30	2.12		1.73	12
Zr	101		122	10												

Table 2. (continued)

	***M.I 12 plg1 th 1	RSD (%) $n = 5$	***M.I 13 plg1 th 1	RSD (%) $n = 5$	*M.I 1 plg2 th 1	RSD (%) $n = 5$	***M.I 6 plg3 th 1	***M.I 7 plg3 th 1	M.I 1 plg4 th 1	***M.I 1 olv1 th 2	**M.I 1 olv2 th 3	M.I 1 spin 1 th 1	M.I 1 spin 2 th 1
Major (wt%)													
SiO_2	50.27	0.27	50.28	0.25	49.80	0.93	49.91	50.41	50.75	50.41	52.10	48.63	50.19
TiO_2	1.06	1.65	1.05	2.76	0.89	4.9	1.02	0.90	1.62	1.03	1.52	1.21	0.84
Al_2O_3	14.36	0.81	13.97	1.39	13.80	0.74	14.35	14.07	14.43	17.45	20.02	17.45	15.79
FeO_{tot}	8.07	1.47	8.50	1.81	8.90	1.5	8.58	8.80	10.36	7.83	6.83	9.77	7.57
MnO	0.17	7.76	0.16	3.51	0.16	21	0.18	0.17	0.26	0.14	0.18	0.19	0.15
MgO	10.70	1.06	10.82	1.56	10.30	0.94	10.58	10.61	7.35	7.46	2.88	6.70	9.29
CaO	11.73	1.38	11.72	1.90	11.70	0.75	11.85	11.78	11.25	13.56	14.92	10.81	12.64
Na_2O	2.10	2.82	2.02	2.56	2.00	3.4	2.21	2.06	2.45	2.44	3.03	2.60	2.24
P_2O_5	0.17	10.35	0.16	5.42	0.29	13	0.19	0.16	0.19	0.19	0.38	0.21	0.19
K_2O	0.08	5.89	0.09	6.76	0.11	5.4	0.10	0.09	0.24	0.06	0.06	0.16	0.18
Mg value	0.70		0.69		0.67		0.69	0.69	0.56	0.63	0.43	0.55	0.69
Total	98.76		98.83		98.06		99.05	99.09	99.20	100.57	102.24	100.22	100.21
Trace (ppm)		$n = 2$		$n = 2$		$n = 4$							—
Ba	12.4	16	12.6	3.4	19.8	20	20.8	23.7	—	17.4	14.7	—	—
Ce	5.71	16	5.21	3.4	6.52	17	6.63	5.44	—	6.89	9.85	—	—
Dy	2.68	9.1	2.29	3.5	2.02	15	3.90	2.26	—	3.34	4.81	—	—
Er	1.55	7.2	1.37	1.5	1.35	20	2.34	1.24	—	1.69	3.70	—	—
Eu	0.83	14	0.70	8.5	0.76	19	0.99	0.81	—	1.04	1.27	—	—
Hf	1.16	18	1.12	3.4	1.09	11	1.43	0.92	—	1.24	—	—	—
La	1.62	14	1.54	1.0	2.53	15	2.22	1.84	—	2.42	3.58	—	—
Nb	1.22	6.6	1.05	3.9	2.27	17	2.58	1.41	—	1.79	1.53	—	—
Nd	5.16	7.8	4.94	2.5	4.74	16	5.90	4.04	—	5.94	11.7	—	—
Pb	0.36	22	0.34	3.4	—	—	0.41	0.46	—	1.27	—	—	—
Rb	1.22	21	0.99	4.8	1.16	>30	3.25	2.24	—	b.d	0.92	—	—
Sm	1.91	20	1.59	0.6	1.54	20	2.34	1.60	—	2.33	2.46	—	—
Sr	95.7	9.0	90.0	4.8	89.2	14	106	112	—	117	172	—	—
Ta	0.10	1.5	0.06	2.4	0.12	14	0.16	0.08	—	0.11	—	—	—
Th	0.07	7.3	0.06	29	0.22	25	0.21	0.16	—	0.97	—	—	—
U	b.d	>30	0.03	19	0.05	>30	0.06	0.05	—	0.06	—	—	—
Y	15.1	6.5	13.5	1.3	12.5	8.3	20.3	11.6	—	17.2	28.1	—	—
Yb	1.58	19	1.46	1.9	1.20	20	2.27	1.34	—	2.2	4.4	—	—
Zr	45.0	10	40.9	1.8	42.0	7.7	54.1	31.6	—	46.8	67.9	—	—

Table 2. (continued)

	*M.I 1 plg 1 th 1	*M.I 2 plg1 th 1	**M.I 3plg1 th 1	**M.I 4 plg1 th 1	***M.I 5 plg1 th 1	***M.I 10 plg1 th 1	***M.I 12 plg1 th 1	***M.I 13 plg1 th 1	*M.I 1 plg2 th 1	***M.I 1 olv1 th 2	**M.I 1 olv2 th 3
Major (wt%)											
SiO_2	50.38	50.10	50.06	50.12	50.35	50.67	50.54	50.50	50.44	49.41	48.71
TiO_2	0.74	0.98	0.85	0.88	0.85	0.83	0.95	0.93	0.79	0.94	1.18
Al_2O_3	16.34	16.34	16.44	16.45	16.49	16.40	16.58	16.39	16.34	15.97	15.89
FeO_{tot}	7.74	7.60	7.83	7.70	7.46	7.50	7.22	7.55	7.94	8.12	8.97
MnO	0.14	0.14	0.10	0.14	0.15	0.15	0.15	0.14	0.14	0.16	0.24
MgO	9.42	9.39	9.68	9.57	9.74	9.63	9.59	9.59	9.21	10.29	9.98
CaO	12.50	12.71	12.38	12.38	12.28	12.3	12.30	12.31	12.39	12.40	11.95
Na_2O	2.06	2.08	2.01	2.08	2.14	2.03	2.16	2.09	2.09	2.23	2.35
P_2O_5	0.29	0.26	0.25	0.27	0.16	0.12	0.15	0.14	0.25	0.18	0.29
K_2O	0.09	0.10	0.08	0.09	0.07	0.08	0.07	0.08	0.10	0.05	0.05
Mg value	0.69	0.69	0.68	0.69	0.70	0.69	0.70	0.69	0..67	0.69	0.67
Trace (ppm)											
Ba	11.7	12.0	15.4	13.8	16.1	18.3	11.2	11.3	17.7	16.0	11.8
Ce	4.56	3.97	5.62	5.59	6.98	6.48	5.12	4.62	5.77	6.34	7.88
Dy	2.54	1.95	3.05	2.84	2.80	2.58	2.38	2.01	1.79	3.07	3.85
Er	1.39	1.22	2.06	2.25	1.62	1.48	1.38	1.21	b.d	1.55	2.96
Eu	0.76	0.77	0.82	0.88	0.80	0.86	0.76	0.63	0.70	0.96	1.01
Hf	1.20	0.82	1.27	—	0.89	1.11	1.03	0.99	0.96	1.14	—
La	1.68	1.34	1.56	1.91	2.34	2.01	1.47	1.38	2.26	2.23	2.86
Nb	0.98	0.72	1.23	1.37	2.78	1.05	1.08	0.93	b.d	1.65	1.22
Nd	4.28	3.75	5.42	5.81	4.95	5.77	4.60	4.37	4.21	5.46	9.4
Pb	—	—	0.38	—	0.36	0.39	0.34	0.32	—	1.17	—
Rb	0.93	b.d	1.49	1.63	2.54	1.91	1.42	1.24	1.14	b.d	0.73
Sm	1.64	1.26	1.78	2.01	1.68	1.92	1.71	1.40	1.37	2.14	1.97
Sr	104	100	111	107	106	112	103	99	101	108	137
Ta	0.08	0.04	0.08	—	0.15	0.07	0.09	0.06	b.d	0.10	—
Th	0.17	0.03	0.08	—	0.16	0.08	0.06	0.06	0.19	0.89	—
U	0.14	0.08	0.03	—	0.07	0.02	b.d	0.02	b.d	0.06	—
Y	13.9	12.1	16.8	16.1	15.3	13.5	13.4	11.9	11.0	15.8	22.4
Yb	1.32	1.08	1.87	1.43	1.86	1.54	1.40	1.28	b.d	2.02	3.54
Zr	38.0	30.1	44.1	45.1	35.1	38.4	40.0	36.0	b.d	43.1	54.3

(*) = analyzed by Nd-YAG 266 nm, (**) = analyzed by Excimer 193 nm, (***) = analyzed by Nd-YAG 213 nm. RSD is not shown for n = 1.
(b.d) = below detection; (—) = not determined. M.I = melt inclusion.

Table 3. Representative analysis of minerals by Nd-YAG 213 nm

	plg 1 th 1 pt.1 core	pt.2 core	pt.3 core	pt.4 core	pt.5 core	pt.6 core	pt.7 core	pt.8 core	pt.9 core	pt.10 core	pt.11 core	pt.12 core	pt.13 core	pt.14 core	pt.15 core	pt.16 core	pt.17 rim	plg 2 th 1 core	olv 1 th 2 core	olv 2 th 3 core
Major (wt%)																				
SiO_2	46.81	46.95	46.71	46.90	46.42	46.81	46.80	46.69	46.45	46.48	46.16	46.29	46.21	46.31	46.49	46.50	49.63	45.28	40.80	39.19
Al_2O_3	32.41	32.31	32.55	32.50	32.73	32.50	32.59	32.60	32.81	32.69	32.88	32.85	32.72	32.74	32.84	32.75	28.73	32.25	0.08	0.07
FeO	0.34	0.31	0.27	0.25	0.31	0.34	0.24	0.26	0.28	0.32	0.30	0.29	0.34	0.27	0.27	0.28	0.69	0.32	10.93	11.93
MgO	0.24	0.24	0.20	0.21	0.22	0.22	0.20	0.21	0.19	0.20	0.21	0.19	0.19	0.20	0.18	0.22	0.25	0.21	49.26	47.07
CaO	18.58	18.35	18.83	18.75	18.85	18.66	18.68	18.68	18.77	18.86	19.01	19.01	19.25	19.03	18.84	18.74	14.85	18.67	0.29	0.28
Na_2O	1.55	1.77	1.36	1.32	1.34	1.39	1.45	1.47	1.39	1.36	1.37	1.26	1.23	1.34	1.31	1.44	3.25	1.21	0.02	b.d
P_2O_5	0.03	0.03	0.03	0.04	0.07	0.05	0.03	0.07	0.06	0.04	0.04	0.06	0.05	0.06	0.04	0.03	0.06	0.06	b.d	b.d
K_2O	0.02	0.01	0.02	0.01	0.01	0.01	0.01	0.01	0.01	0.00	0.01	0.01	0.01	0.00	0.02	0.01	0.03	0.01	0.01	0.01
An																				
trace el. (ppm)																				
Ba	3.24	2.21	2.33	1.94	1.69	1.87	1.96	2.37	1.94	2.47	2.42	2.04	2.36	2.30	2.48	2.70	20.20	1.87	—	1.88
Ce	0.36	0.19	0.24	0.22	0.28	0.24	0.18	0.22	0.30	1.05	0.20	0.21	0.22	0.27	0.34	0.31	0.62	0.24	—	0.02
Co	3.24	3.97	2.94	3.78	3.94	3.99	4.03	3.81	2.79	3.73	3.90	3.51	3.76	4.14	3.81	3.73	8.14	4.45	—	31.3
Cr	b.d	60.7	b.d	b.d	b.d	b.d	26.1	21.3	b.d	b.d	14.9	b.d	b.d	b.d	b.d	b.d	199	b.d	—	66.8
Dy	b.d	0.03	0.01	0.04	b.d	0.05	0.04	0.03	b.d	b.d	0.04	0.01	b.d	0.05	0.07	0.04	0.06	0.14	—	0.02
Er	b.d	b.d	0.01	b.d	b.d	0.03	b.d	b.d	b.d	0.02	0.02	0.03	0.01	b.d	0.01	b.d	0.07	b.d	—	0.01
Eu	0.18	0.17	0.21	0.16	0.13	0.18	0.19	0.48	0.16	0.15	0.18	0.20	0.16	0.15	0.14	0.15	0.37	0.22	—	0.02
Gd	b.d	b.d	0.13	0.14	b.d	0.11	0.02	0.01	0.05	0.06	0.06	0.03	0.08	0.12	0.09	0.05	0.59	0.35	—	0.13
Hf	b.d	0.01	0.04	b.d	0.01	0.01	b.d	b.d	b.d	0.16	b.d	0.04	0.07	b.d	b.d	b.d	0.17	0.03	—	0.02
La	0.09	0.06	0.15	0.07	0.07	b.d	0.07	0.13	0.20	0.01	b.d	0.07	0.10	b.d	0.06	0.07	0.82	0.31	—	0.09
Nb	b.d	0.04	0.02	0.32	0.04	0.04	b.d	b.d	b.d	0.01	0.01	b.d	b.d	0.01	b.d	1.02	0.06	b.d	—	0.04
Nd	0.12	0.14	0.16	0.18	0.14	0.23	0.06	b.d	0.14	0.11	0.14	0.12	0.18	0.17	0.07	0.30	0.34	0.32	—	0.04
Pb	0.84	0.02	0.42	0.26	b.d	b.d	0.04	b.d	0.20	b.d	b.d	b.d	b.d	0.01	0.09	0.04	0.13	b.d	—	0.24
Rb	0.83	1.38	1.62	1.27	1.62	2.04	1.93	1.14	3.05	1.60	1.97	2.21	3.11	2.28	2.29	0.57	4.95	0.96	—	0.89
Sc	7.51	11.9	7.67	10.4	10.2	6.88	9.67	9.83	7.13	11.9	14.3	10.1	10.8	12.3	12.0	10.7	24.7	4.50	—	11.5
Sm	b.d	0.02	0.06	0.01	0.09	b.d	0.07	0.02	0.01	0.06	b.d	0.06	b.d	0.09	0.02	0.03	0.37	0.14	—	0.06
Sr	187	169	181	168	159	184	175	168	165	165	166	169	171	183	172	180	212	188	—	0.38
Ta	b.d	b.d	b.d	b.d	b.d	b.d	b.d	0.06	0.03	b.d	b.d	0.01	b.d	b.d	b.d	0.01	0.02	b.d	—	0.01
Th	b.d	0.01	0.01	0.01	0.01	b.d	b.d	b.d	b.d	b.d	b.d	b.d	b.d	0.00	0.00	b.d	b.d	b.d	—	b.d
Ti	137	116	123	109	108	97	88	92	84	92	101	92	102	109	112	114	393		—	22.2
U	b.d	0.04	b.d	b.d	b.d	b.d	b.d	b.d	b.d	b.d	b.d	b.d	b.d	b.d	b.d	b.d	b.d	b.d	—	b.d
V	3.08	2.32	2.32	2.26	2.54	2.64	2.25	2.00	1.91	2.41	2.17	2.34	2.66	3.05	3.09	3.01	5.26	2.43	—	1.73
Y	0.12	0.04	0.09	0.10	0.10	0.05	0.10	0.04	0.04	0.09	0.04	0.14	0.04	b.d	0.07	0.13	0.20	0.01	—	0.13
Yb	0.02	b.d	0.02	0.03	b.d	0.02	b.d	b.d	b.d	0.03	0.04	b.d	b.d	b.d	b.d	0.02	0.01	b.d	—	0.04
Zr	0.01	b.d	b.d	0.05	0.13	b.d	b.d	b.d	0.18	b.d	0.11	b.d	b.d	b.d	0.01	0.03	2.29	b.d	—	1.23

pt.1 to pt.17 represent the traverse analysis of a single plg phenocryst.
(b.d) = below detection; (—) = not determined.

Table 4. Analysis of the same basaltic glass by different laser systems

glass th 1 (n = 10)	Ba	Ce	Dy	Er	Eu	La	Nb	Nd	Sm	Sr	Y	Yb	Zr
Nd-YAG 213 nm	46	16	4.9	2.9	1.4	5.5	5.4	11.2	3.7	119	26	2.9	88
Nd-YAG 266 nm	36	14	4.2	2.8	1.3	4.5	4.6	10.7	3.5	107	26	2.5	86
Excimer 193 nm	43	16	6.4	3.0	1.5	6.0	6.8	11.9	4.2	120	29	3.1	93

The elemental abundances are expressed in ppm.

not display a correlation with the mineral composition and are not arranged along fractures suggesting to be primary (Schiano, 2003). They are glassy, homogeneous and sometimes contain small shrinkage bubbles (Schiano, 2003). Often they are surrounded by an albitic (An 69–73%) plagioclase overgrowth and they do not contain daughter mineral phases.

The olivine phenocrysts are generally large (300–1000 μm), often euhedral, with high Forsterite content (85–90%) and unzoned, rarely contain small melt inclusions (10–30 μm) that are always round, glassy and homogeneous. Olivine microphenocrysts can be observed as small (<200 μm) and euhedral individuals, lower in Forsterite (79–82%), without zoning and showing rare melt inclusions.

The spinels phenocrysts are generally small (20–150 μm) and round, they have a very variable Cr number (27–53) and Mg number (45–72), rarely trapped small melt inclusions (5–20 μm) that are glassy and round. The most primitive spinels are included in the large plagioclase phenocrysts and do not have zoning, whereas the more evolved spinels are embedded in the groundmass and display a normal zoning.

Techniques of Analysis

The three tholeiites object of this melt inclusions study were analyzed by XRF (Philips PW 1480) at the University of Studies of Florence to determine SiO_2, Al_2O_3, TiO_2, FeOtot, MnO, CaO, K_2O and P_2O_5. Na_2O and MgO were determined by atomic absorption spectrophotometry (AAS) while FeO and Fe_2O_3 were determined by a titration with $K_2Cr_2O_7$ (0.07 N) of a solution containing the previously dissolved samples by acid attack. The loss on ignition (LOI) was determined by weight differences before and after heating the samples at 950°C for a time sufficient to reach the constant weight (Table 1).

Around 20 large melt inclusions (30–400 μm) trapped in plagioclases and olivines were analyzed by Laser Ablation-Inductive Coupled Plasma Mass Spectrometer (LA-ICPMS) VG PQ3, coupled with two types of Nd-YAG UV laser systems (266 nm and 213 nm) at the Earthquake Research Institute, The University of Tokyo, to determine 19 trace elements (Ba, Ce, Dy, Er, Eu, Hf, La, Nb, Nd, Pb, Rb, Sm, Sr, Ta, Th, U, Y, Yb and Zr) (Table 2). As for Nd-YAG 266 nm, the best setting for the melt inclusions was obtained using a medium size laser beam, which produced craters of nearly 40 μm in diameter and 70–100 μm depth. The laser repetition rate was 6 Hz, with 50 seconds of ablation time and 3 seconds of pre-ablation time. As for Nd-YAG 213 nm, the analysis were performed using a laser beam of 30 μm in diameter, a repetition rate of 6 Hz and ablation time of 30 seconds with 3 seconds of pre-ablation. A few melt inclusions were analyzed at the Tokyo Institute of Technology using an ICPMS coupled with Excimer laser (193 nm wavelength), which is able to produce crater pits of only 15–20 microns in diameter in glasses and melt inclusions (Iizuka and Hirata, 2004). The ablation time and the repetition rate were set respectively to 20 seconds and 5 Hz and the pre-ablation time was set to 3 seconds. For internal normalization ^{44}Ca and ^{25}Mg were selected because of their abundant concentration in MORB and its ease of analysis by EPMA. A standard reference material (NIST SRM 610), based on an evaluation of the abundance data in the literature (Pearce *et al*., 1997), was used for calibration, in addition to test of sensitivity, standard deviation and accuracy of the analytical procedures. The details of the analytical procedure basically follow Orihashi and Hirata (2003) and Orihashi *et al*., (2003). After 266 nm ablation, the samples were step-wise ground, and we confirmed that the ablated materials were completely inside the melt inclusions, ensuring no contamination from the host plagioclase. The analytical results obtained from craters that penetrated host plagioclase were discarded. This grinding technique, to ensure the absence of contamination by the host plagioclase, is destructive, while making it possible to see the shape of the melt inclusion and crater pits in 3-D perspective. The results of melt inclusion analysis were acceptable for most of the elements with RSD < 5% for Sr and Zr; <10% for La, Ce, Nb, Y, <20% for Ba, Er, Eu, Dy, Pb and Sm. Only the heavier elements Ta, Th and U generally did not give good results with RSD > 30%, whereas Hf and Rb gave different results depending on the used instruments (Table 2).

The host mineral phases were analyzed by 213 nm Nd-YAG to determine 25 trace elements (Ba, Ce, Co, Cr, Dy, Er, Eu, Gd, Hf, La, Nb, Nd, Pb, Rb, Sc, Sm, Sr, Ta, Th,

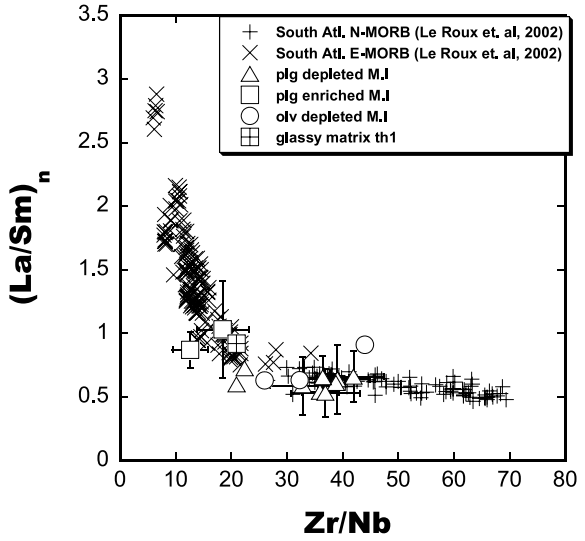

Fig. 3. Zr/Nb vs. $(La/Sm)_n$ plot for melt inclusions (this work) and MORBs (Le Roux et al., 2002a). plg = plagioclase; olv = olivine; M.I = melt inclusions.

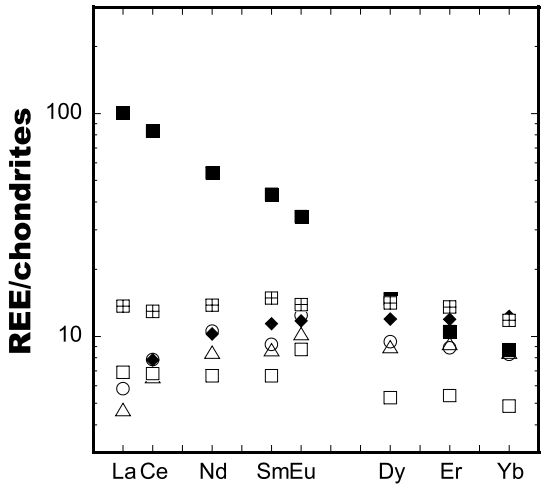

Fig. 4. REE patterns for M.I compared with average N-MORB and average OIB (Sun and McDonough, 1989). Filled square = average OIB; filled diamond = average N-MORB; the other symbols as in Fig. 3.

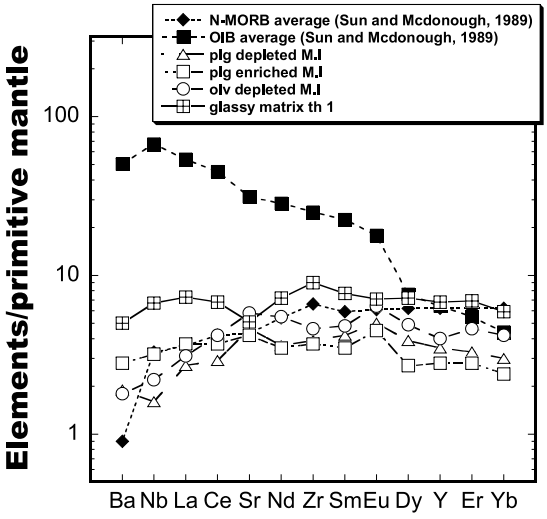

Fig. 5. Spider diagrams for M.I compared with average N-MORB and average OIB (Sun and McDonough, 1989).

Ti, U, Y, Yb and Zr) and the results were acceptable (RSD < 20%) for a significant number of elements (Ba, Ce, Co, Eu, Sr, Ti, and V for plagioclase, Ba, Dy, Hf, Rb, Sc, Sr, Y, Yb and Zr for olivines) (Table 3).

The melt inclusions in olivine and spinels were quite small (<30 μm) then most of them were not well analyzed by LA-ICPMS. In all the analysis performed by the three instruments a systematic bias was not observed for any element (Table 4), therefore the data could be used as a unique set.

Minerals, glassy matrices and melt inclusions were analyzed by EPMA for the major elements at the Earthquake Research Institute (Tables 2 and 3).

RESULTS

Major elements

The melt inclusions trapped in large plagioclase core phenocrysts display a quite constant composition within a single crystal and among different crystals and they are quite primitive (Mg value 0.67–0.70), whereas the melt inclusions trapped in the plagioclase rims or in the sodic microlites have a more evolved composition (Mg value 0.52–0.56) that is similar to the glassy matrix compositions (0.51–0.54) (Table 2).

The melt inclusions included in the forsterite rich olivines (Fo 85–90) of th 3 have a very low MgO (2.43–2.88 wt%) and very high Al_2O_3 (19.47–20.02 wt%), plotting very far from the primitive basaltic glasses (Le Roux *et al.*, 2002a), whereas the melt inclusions trapped in olivine of th 2 plot nearer (Fig. 7, Table 2).

The melt inclusions trapped in primitive spinel phenocrysts display high Mg value (0.63–0.69) and a quite constant composition both within single crystals and among different crystals plotting very near to the basaltic glasses. The melt inclusions trapped in Fe rich spinels (Mg value 0.55–0.62) are different from the basaltic glasses, having higher Al_2O_3, Na_2O, TiO_2 and FeO and lower CaO and MgO (Table 2).

Trace elements

Most of the melt inclusions trapped in the plagioclase core phenocrysts exhibit a depleted composition and could

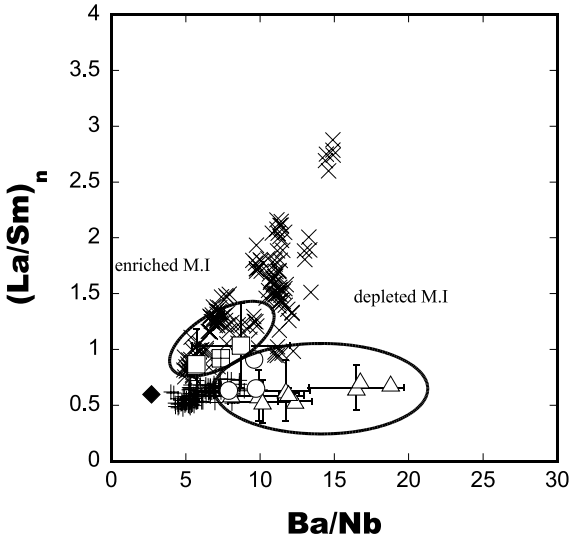

Fig. 6. Ba/Nb vs. $(La/Sm)_n$ plot for M.I compared with the South Atlantic basaltic glasses (Le Roux et al., 2002a). The symbols are as in Fig. 5.

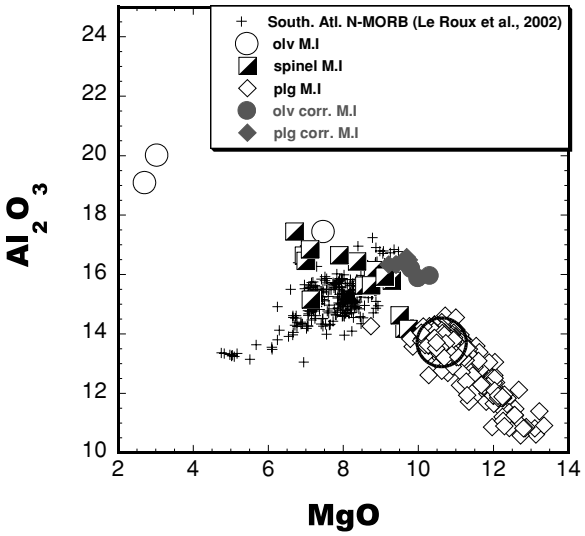

Fig. 7. MgO vs. Al_2O_3 plot for M.I (this study) and MORBs (Le Roux et al., 2000a). The filled diamonds and filled circles represent the melt compositions corrected for the post entrapment crystallization. The olivine M.I (empty circles) were all corrected, whereas only large plg M.I analyzed by LA-ICPMS that plot within the large empty circle were corrected.

be classified as N-MORB type, having $(La/Sm)_n < 0.75$, a few of them can be classified as E-MORB type, having $(La/Sm)_n > 0.75$, and trace element ratios varying significantly among melt inclusions contained in the same hand specimen. The melt inclusions trapped in a highly calcic plagioclases of the same sample (th 1) have generally a depleted composition with $(La/Sm)_n$ 0.54–0.72 and Zr/Nb 22–44, but some of them have very different composition with $(La/Sm)_n$ = 0.79–1.09 and Zr/Nb = 12–18 (Fig. 3). The glassy matrix of th 1 has a composition quite similar to the enriched melt inclusions, whereas the olivine primitive melt inclusions are chemically depleted, being similar to the depleted melt inclusions in plagioclase.

The REE patterns of the depleted melt inclusions in plagioclase and olivine show depletion of LREE relatively to the HREE, which are similar to average N-MORB (Sun and McDonough, 1989) while the enriched melt inclusions in plagioclase and the glassy matrix show a typical E-MORB trend with no depletion of LREE relatively to HREE (Fig. 4). In the spider diagram the melt inclusions have a pattern clearly different from the N-MORB average (Sun and McDonough, 1989) in showing positive anomalies of Sr and Eu, whereas the glassy matrix of th 1, more evolved than melt inclusions, shows negative anomalies for Sr and Eu (Fig. 5). The depleted melt inclusions (N-MORB type) have anomalously high Ba/Nb ratios (8–18), much higher than in average N-MORB (nearly 3) and are not positively correlated with $(La/Sm)_n$ as in E-MORB (Douglass *et al.*, 1995). The enriched melt inclusions and the matrix glass (E-MORB type) have lower Ba/Nb and higher $(La/Sm)_n$ (Fig. 6).

The plagioclase phenocrysts have a very homogeneous composition in trace elements, as evidenced by the traverse analysis (Table 3) and no significant difference exists among crystals. The olivine phenocrysts are also very homogeneous in major and trace elements, without significant zoning.

Discussion and Concluding Remarks

In order to discuss the geochemistry and the petrogenesis of MORBs in terms of melt inclusions chemistry, it is necessary to consider the effects of secondary processes, such as the post-entrapment crystallization of the host mineral and the elemental diffusion.

Post entrapment crystallization effect

Post-entrapment crystallization is commonly observed in plagioclase phenocryst melt inclusions (Nielsen *et al.*, 1995; Sinton *et al.*, 1993) and it is a very common secondary process (Schiano, 2003). In order to evaluate the effect of this process, the composition of the South Atlantic glasses (Le Roux *et al.*, 2002a) and that of the melt inclusions (this study) were plotted together (Fig. 7). In terms of major elements the plagioclase melt inclusions differ from the primitive South Atlantic MORB glasses, due to the post-entrapment crystallization of the plagioclase host. In fact, as a result of post-entrapment crystallization, the melt inclusions became depleted in CaO and Al_2O_3 and enriched in MgO, FeO, TiO_2 and other plagioclase incompatible elements, relative to their val-

ues in the original trapped melt (Table 2). The post entrapment effect is highly variable among different melt inclusions and is more important in the smaller melt inclusions (<10–20 μm). The overgrowth of the plagioclase around the melt inclusions is occasionally observed in the EPMA backscattered images as a thin rim, which is not always possible to be analyzed with EPMA, but it is found to be quite sodic (An 73% on average) and could be used for the correction if the volume of the overgrowth is estimated. Nevertheless in order to apply a systematic correction to all the melt inclusions we prefer to apply the thermodynamic algorithm based on the self-consistent thermodynamic model used in MELTS software (Kress and Ghiorso, 2004). Firstly, using the well known relation $[Fe/Mg]_{sol}/[Fe/Mg]_{liq} = 0.30$ (Roeder *et al*., 1970) we applied the correction for the olivine phenocryst melt inclusions in order to constrain the conditions (*P*, *T*) also for the plagioclase phenocryst melt inclusions correction. We initially supposed that the plagioclase phenocrysts grown near the cotectic with the olivine phenocrysts and we applied the same conditions also for the plagioclase melt inclusions correction in the algorithm. As results we obtained that the corrected olivine and plagioclase melt inclusions match closely the most primitive basaltic glasses (Le Roux *et al*., 1989) an important clue for the goodness of the correction. According to the results, the magnitude of the corrections is very small (6–12%) with the exception of olivine melt inclusions of th 3 (nearly 20%) and therefore the trace element abundances are only slightly modified by the host overgrowth (Table 2). In terms of trace elements, we corrected the plagioclase melt inclusions considering the trace element abundances of their hosts, whereas we corrected the olivine melt inclusions by a dilution. We found that, not only in terms of incompatible element ratios the geochemical significance is preserved after correction, but also the absolute abundances are not significantly modified, being generally well within the analytical error of the instruments.

Diffusion effect

The melt inclusions could be modified by the diffusion of the elemental species from the host lavas through the host mineral and a significant example of this process is represented by the chromite inclusions and the host olivines that were observed to re-equilibrate with their host basalt in a lava lake of Kilauea (Scowen *et al*., 1991). As in the case of chromites, also melt inclusions could re-equilibrate with the host basalt by cations diffusion through the host plagioclase, however in our case some evidence suggests that the re-equilibration is not an important process. In the case of Kilauea the olivines and their trapped chromites show a compositional gradient, whereas the plagioclase phenocrysts show a sharp sodic rim and the melt inclusions do not show any

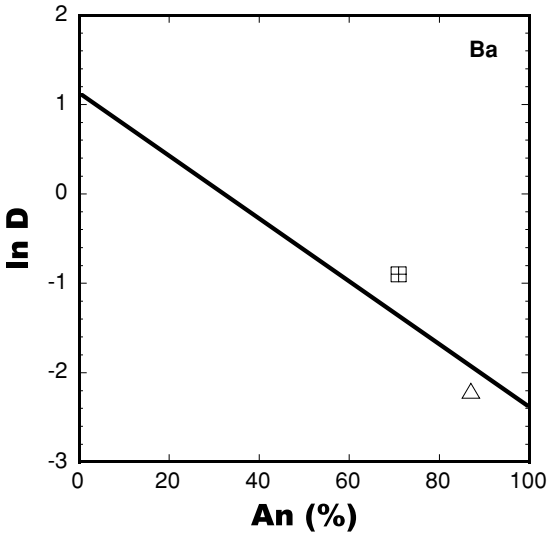

Fig. 8. Ln $D^{Ba}_{(plg\ core/M.I)}$ and ln $D^{Ba}_{(plg\ rim/groundmass)}$ vs. An (%) content. The empty triangle represents ln $D^{Ba}_{(plg\ core/M.I)}$ while the square represents ln $D^{Ba}_{(plg\ rim/groundmass)}$. The straight line is the An (%) vs. ln D^{Ba} correlation line derived from experimental data (Bindeman et al., 1998).

compositional-distributional correlation along the large cores. In a recent study Bindeman *et al*., (1998) made available a large dataset of plagioclase partition coefficients in equilibrium with a basaltic liquid. The major and trace elements concentrations for plagioclase rims and cores together with the data of the groundmass and melt inclusions were used to check if the partition coefficients of these MORB fit with the data determined experimentally. It was found that there is a good agreement between the partition coefficients determined experimentally and our data. Particularly $D^{Ba}_{(plg/liquid)}$, which is strong dependent from plagioclase An content, suggests that plagioclase rims are in equilibrium with the groundmass, whereas the plagioclase cores should be in equilibrium with the melt inclusions (Table 5, Fig. 8). These results also show the absence of a gradient and consequently are against the occurrence of a re-equilibration of melt inclusions with the groundmass.

Petrogenesis of the Shona MORB

In the recent years the South Atlantic MORB (40–55°S) have been extensively studied to clarify the geochemical character of these rocks (Le Roux *et al*., 2002a) and to explain in detail the process of partial melting of the mantle (Le Roux *et al*., 2002b). The geochemical domains were clearly distinguished by trace elements, isotopes and oceanic floor morphology and structures. It was found that the presence of chemically enriched MORB is related to two hot spots, the Discov-

Table 5(a). Partition coefficients (D) for plg rim/glass and for plg core/M.I

	plg 1 th1 rim	glass	ln *D*	plg 1 th 1 core	mi 5	ln *D*
Major (wt%)						
SiO_2	49.81	50.80	–0.02	46.80	52.12	–0.11
Al_2O_3	27.80	13.30	0.74	31.59	16.36	0.66
FeO	0.68	10.60	–2.75	0.24	7.68	–3.47
MgO	0.25	7.10	–3.33	0.20	9.99	–3.92
CaO	14.81	11.10	0.29	18.68	13.22	0.35
Na_2O	3.20	2.50	0.25	1.45	2.10	–0.37
P_2O_5	0.05	0.30	–1.88	0.03	0.16	–1.69
An	71			87		
Trace el. (ppm)						
Ba	17.7	44.9	–0.9	1.99	18.0	–2.2
Ce	0.66	15.6	–3.2	0.18	7.89	–3.8
Eu	0.39	1.53	–1.4	0.19	0.70	–1.3
Sr	228	122	0.6	177	97.7	0.6
Ti	413	10050	–3.2	89.7	5438	–4.1

Table 5(b). Partition coefficients (D) for olv core/M.I

	olv 2 th 3	M.I olv 2 th 3	ln *D*
Major el. (wt%)			
TiO_2	0.012	1.23	–4.63
FeO	12.02	8.40	0.36
MnO	0.19	0.17	0.14
MgO	46.84	9.80	1.56
CaO	0.26	9.75	–3.64
Fo	87		
Trace el. (ppm)			
Ba	1.88	12.4	–1.89
Dy	0.02	3.60	–5.22
Eu	0.02	1.08	–3.98
Sc	11.5	25.7	–0.80
Sm	0.06	2.12	–3.64
Sr	0.38	123	–5.79
V	1.73	189	–4.69
Y	0.13	18.1	–4.91
Zr	1.23	50.8	–3.72

ery and the Shona (Douglass *et al*., 1995) and that N-MORBs in this region differ from the global average N-MORB because of an old crustal component in the regional shallow mantle. The Shona hot spot is considered to be a ridge centered hot spot, therefore the plume component is probably efficiently mixed with the depleted asthenospheric mantle to explain the absence in the area of highly enriched MORB (Le Roux *et al*., 2002b), provided that the extreme component of the Shona plume is still unknown. The depleted component of the Shona MORB, and more generally the depleted components of the South Atlantic and Indian mantle are anomalous if compared with other regions. In fact the local N-MORB have exceptionally high Ba/Nb (4–9), La/Nb (1.2–2.4), K/Nb (>1), and have more radiogenic Pb and Sr isotopes and less radiogenic Nd than typical N-MORB (Le Roux *et al*., 2002a; Rehkamper and Hofmann, 1997).

In the specimen th 1 melt inclusions of both N-MORB and E-MORB types were found in this study. Both kinds of melt inclusions exhibit almost the same Mg value (0.67–0.69) and the N-MORB type supposedly preserved a near primary end-member source. The N-MORB melt inclusions have unusually high Ba/Nb (8–18), high Zr/Nb (22–44), low $(La/Sm)_n$ (0.54–0.72) and positive anomalies of Sr and Eu (1.00–1.6). High Ba/Nb ratios were already found in the South Atlantic and Indian N-MORB (Le Roux *et al*., 2002a; Rehkamper and Hofmann, 1997) but the extreme ratios obtained in this study sug-

gest that the Shona regional depleted mantle should contain a geochemical component, displaying particularly high Ba content. This component could be represented by marine sediments (Plank and Langmuir, 1998) that were entrained during the subduction process antecedent to the opening of the ocean basin (Grunow, 1996; Unrug, 1996). The melt inclusions with high Ba/Nb ratio are depleted: this suggests that this anomalous geochemical component is present only in the depleted shallow mantle and not in the plume component.

Positive Sr and Eu anomalies are very rare in MORB and are generally explained by the partial melting of a plagioclase lherzolite (Gurenko and Chaussidon, 1995), but for the Shona ridge the melting conditions derived by Le Roux *et al*., (2002b) do not favor this hypothesis. By using the equations from Niu and Batiza (1991) we found that the Shona MORB should have been generated at a range of pressure of 20–13 Kbar: these conditions are against the presence of plagioclase in the peridotite, a phase that is stable at lower pressure (<10 Kb) (Presnall *et al*., 2002). Another possible explanation is the remelting of gabbroic rocks inside the magma chamber (Tronnes, 1990). However as in the studied rocks, petrographic evidence of this process, such as inverse zoning or corrosion of the plagioclases or other minerals, are absent, this explanation can be rejected. The diffusion of Sr and Eu through the plagioclase could determine an enrichment of these elements in the re-equilibrated melt inclusions. But we already observed that the partition coefficients $D^{i}_{(plg/melt)}$ and the preservation of a sharp zoning of the plagioclases do not suggest re-equilibration with the host lava and straightforwardly the olivine melt inclusions show similar Sr and Eu anomalies (Fig. 5).

According to the models proposed by Le Roux *et al*., (2002a) and by Rehkamper and Hofmann (1997), one possible source of Sr and Eu positive anomalies could be represented by a recycled component. Assuming that the recycled component is composed by the altered oceanic crust and pelagic sediments, the high Sr and Eu could be caused by the partial melting of recycled gabbroic material of the subducted oceanic crust (Barrat *et al*., 2003; Sobolev *et al*., 2000). In our samples Sr and Eu anomalies are common in the E-MORB and N-MORB, thus we suggest that the recycling of crust material, if occurred, should have affected both types of MORB. An important question is: why the presence of Sr and Eu anomalies has not been noticed in other MORBs from the same domain? Most of the studies involved MORB glasses that were not as primitive as the melt inclusions of this study. Therefore we argue that the positive Sr and Eu anomalies were probably present in the primary magmas, but were obscured during magmatic differentiation in which crystallization of plagioclase produces negative Sr and Eu anomalies in evolved glasses, due to the relative compatibility of these two elements (Dunn and Senn, 1994). This conclusion is consistent with the presence of positive Sr and Eu positive anomalies in the most primitive glasses of the N-MORB of the Central Indian Ridge (C.I.R) (Rehkamper and Hofmann, 1997). The enriched melt inclusions (E-MORB) and the glassy groundmasses probably do not represent the Shona enriched end member component, because the Shona basalts are not as high in $(La/Sm)_n$ as other worldwide plume components. It is probable, as also suggested by Le Roux *et al*., (2002a) that the mildly enriched melts (E-MORB) sampled in the Shona ridge as melt inclusions, represent a mixing of enriched melts, derived from the Shona plume component, and more depleted melts, derived from the shallow mantle.

E-MORBs and N-MORBs

The contemporary presence of E-MORB and N-MORB melts seems to be a fairly common character of worldwide MORB and it is made particularly evident by the increased melt inclusion studies. In the above discussion we considered that the E-MORB and N-MORB are derived by the partial melting of a different mantle source, but we also should consider that recent studies on MORB show that geochemical heterogeneities in narrow area of sampling could be explained by the partial melting of a unique mantle source (Sims *et al*., 2002; Jull *et al*., 2002). If two different systems of melt supply contemporary exist, one system being composed of high porosity channels that could not permit the melts to re-equilibrate with the mantle residual phases and another one made of low porosity channels that permits the re-equilibration, we could, consequently, have the preservation of two different type of melts in the basalts, that could resemble N-MORB and E-MORB melts. Nevertheless the preexisting data of long time decay isotopes (Nd, Sr, Hf, etc.) from the South Atlantic Ocean (Le Roux *et al*., 2002a) show that in this region the trace elements and isotopes have a strong correlation, indicating that E-MORB and N-MORB melts of this study should be the result of different sources partial melting, one source being represented by the depleted shallow mantle, supposedly contaminated by old crustal material and another one being represented by the Shona plume.

On considering the presence of E-MORB and N-MORB in the same basaltic rocks, we infer that the primary melts derived from the mantle partial melting should not have been efficiently mixed during their upwelling inside the mantle. In the crust, where the plagioclase phenocrysts have grown, E-MORB and N-MORB were preserved as plagioclase melt inclusions. The two types of melt inclusions were trapped in plagioclase phenocrysts, which are apparently indistinguishable, because they have the same high calcic composition, same

texture and the same melt inclusions distribution, so the plagioclase phenocrysts that trapped different melts may have grown physically separated, for example in different conduits while experiencing the same conditions of temperature and pressure. Another possible explanation is that the plagioclase phenocrysts have grown in the same magma chamber, but the feeding magmas were not able to mix rapidly and some geochemical differences could have been preserved particularly in the most primitive magmas.

The sample data set of this study shows that the primitive melt inclusions are mostly of N-MORB type, whereas the glassy matrices and the Shona basaltic glasses (Le Roux *et al*., 2002a) are all mildly E-MORB, suggesting that the magmas are mixed at least in the late stages of differentiation, before their effusion. While the N-MORB melt inclusions seem to well represent the extreme depleted end-member of Shona basalts, E-MORB melt inclusions and E-MORB Shona glasses (Le Roux *et al*., 2002a) do not seem to represent any enriched end-member, because of their relatively low $(La/Sm)_n$. The Shona enriched end-member is still not sampled also after this study of primitive melt inclusions, indicating that the highly enriched melts representing the Shona plume end-member, at least, partially mixed with the depleted N-MORB melts within the mantle.

Acknowledgments—E. Bonatti is thanked for sample providing. We thank S. Nakada, S. Nakai and I. Kaneoka. for their comments and we thank T. Wright, H. Iwamori, K. Johnson, T. Kogiso and P. Michael for their constructive review. We are grateful to M. Hamada and A. Furukawa for their assistance in the use of the facilities at the Earthquake Research Institute. We thank M. Ohtsuki for her analytical support on EPMA and finally we thank K. Nonomura for the English checking.

REFERENCES

Andres, M., Toft, J. B. and Schilling, J-G. (2002) Hafnium isotopes in basalts from the southern Mid-Atlantic Ridge from 40°S to 55°S: Discovery and Shona plume-ridge interactions and the role of recycled sediments. *Geochemistry Geophysics Geosystems* **3**(10).

Barrat, J. A., Joron, J. L., Taylor, S., Fourcade, S., Nesbittt, R. W. and Jahn, B. M. (2003) Geochemistry of basalts from Manda Hararo, Ethiopia: LREE-depleted basalts in central Afar. *Lithos* **69**, 1–13.

Bindeman, I. N., Davis, A. M. and Drake, M. J. (1998) Ion microprobe study of plagioclase-basalt partition experiments at natural concentration levels of trace elements. *Geochim. Cosmochim. Acta* **62**(7), 1175–1193.

Carrara, G., Bortoluzzi, G., Zitellini, N., Bonatti, E. and Scientific Party (1997) The Bouvet triple junction Region (South Atlantic): a report on two geological expeditions. *Giornale di Geologia* **59**(1–2).

Cottrell, E., Spiegelman, M. and Langmuir, C. H. (2002) Consequences of diffusive reequilibration for the interpretation of melt inclusions. *Geochemistry Geophysics Geosystems* **3**(5).

Douglass, J., Schilling, J. G., Kingsley, R. H. and Small, C. (1995) Influence of the Discovery and Shona mantle plumes on the southern Mid Atlantic Ridge: Rare earth evidence. *Geophys. Res. Lett.* **22**, 2893–2896.

Douglass, J., Schilling, J. G. and Fontignie, D. (1999) Plume ridge interactions of the Discovery and Shona mantle plumes with the Southern Mid-Atlantic Ridge (40°–55°S). *J. Geophys. Res.* **104**, 2941–2962.

Dunn, T. and Sen, C. (1994) Mineral/Matrix partition coefficients for orthopyroxene, plagioclase and olivine in basaltic to andesitic systems: A combined analytical and experimental study. *Geochim. Cosmochim. Acta* **58**, 717–733.

Grunow, A., Hanson, R. and Wilson, T. (1996) Were aspects of Pan-African deformation linked to Iapetus opening? *Geology* **24**, 1063–1066.

Gurenko, A. A. and Chaussidon, M. (1995) Enriched and depleted primitive melts included in olivine from Icelandic tholeiites: Origin by continuous melting of a single mantle column. *Geochim. Cosmochim. Acta* **59**, 2905–2917.

Iizuka, T. and Hirata, T. (2004) Simultaneous determinations of U-Pb age and REE abundances for Zircons using ArF Excimer laser ablation-ICPMS. *Geochem. J.* **38**, 229–241.

Jull, M., Kelemen, P. B. and Sims, K. (2002) Consequences of diffuse and channelized porous melt migration on uranium series disequilibria. *Geochim. Cosmochim. Acta* **66**(23), 4133–4148.

Kress, V. C. and Ghiorso, M. S. (2004) Thermodynamic modeling of post-entrapment-crystallization in igneous phases. *Journal of Volcanol. Geotherm. Res.* **137**, 247–260.

Le Roux, P. J., Le Roex, A. P., Schilling, J. G., Shimizu, N., Perkins, W. W. and Pearce, N. J. G. (2002a) Mantle heterogeneity beneath the southern Mid-Atlantic Ridge: trace element evidence for contamination of ambient asthenospheric mantle. *Earth Planet. Sci. Lett.* **203**, 479–498.

Le Roux, P. J., Le Roex, A. P. and Schilling, J-G. (2002b) MORB melting processes beneath the southern Mid-Atlantic Ridge (40–55°S): a role for mantle plume derived pyroxenite. *Contrib. Mineral. Petrol.* **144**, 206–229.

Ligi, M., Bonatti, E., Borroluzzi, G., Carrara, G., Fabretti, P., Penitenti, D., Gilod, D., Peyve, A., Skolotnev, S. and Turko, N. (1997) *Science* **276**, Issue 5310, 243–245.

Ligi, M., Bonatti, E., Borroluzzi, G., Carrara, G., Fabretti, P., Gilod, D., Peyve, A., Skolotnev, S. and Turko, N. (1999) Bouvet triple junction in the South Atlantic: Geology and evolution. *J. Geophys. Res.* **104**(B12), 29365–29386.

McKenzie, D. (2000) Constraints on melt generation and transport from U-series activity ratios. *Chem. Geol.* **162**, 81–94.

Michael, P. J., McDonough, W. F., Nielsen, R. L. and Cornell, W. C. (2002) Depleted melt inclusions in MORB plagioclase: messages from the mantle or mirages from the magma chamber? *Chem. Geol.* **183**, 43–61.

Nielsen, R. L., Crum, J., Bourgeois, R., Hascall, K., Forsythe, L. M., Fisk, M. R. and Christie D. M. (1995) Melt inclusions in high-An plagioclase from the Gorda Ridge: an example of the local diversity of MORB parent magmas. *Contrib. Mineral. Petrol.* **122**, 34–50.

Niu, Y. and Batiza, R. (1991) An empirical method for calculating melt compositions produced beneath mid-ocean ridges: application for axes and off-axis (seamounts) melting. *J. Geophys. Res.* **96**, 21753–21777.

Orihashi, Y. and Hirata, T. (2003). Rapid quantitative analysis of Y and REE abundances in XRF glass bead for selected GSJ reference rock standards using Nd-YAG 266 nm UV laser ablation ICP-MS. *Geochem. J.* **37**, 401–412.

Orihashi, Y., Hirata, T., Tani, K. and Yoshida. H. (2003) Rapid and simultaneous determination of multi-element abundances and U-Pb age for zircon crystal using UV laser ablation ICP-MS technique: critical evaluation of the technique with 91500 zircon standard. *J. Min. Petrol. Sci.* **98**, 109–112.

Pearce, N. J. G., Perkins, W. T., Westgate, A., Gorton, M. P., Jackson, S. E., Neal, C. R. and Chenery. S. P. (1997) A compilation of New and Published Major and trace Element Data for NIST SRM 610 and NIST 612 Glass Reference Materials. *Geostand. Newslett.* **21-1**, 115–144.

Plank, T. and Langmuir, C. H. (1998) The chemical composition of subducting sediment and its consequences for the crust and mantle. *Chem. Geol.* **145**, 325–394.

Presnall, D., Gudmundur, H., Gudfinnsson, H. and Walter, M. J. (2002) Generation of mid-ocean ridge basalts at pressure from 1 to 7 GPa. *Geochim. Cosmochim. Acta* **66**, 2073–2090.

Rehkamper, M. and Hofmann. A. W. (1997) Recycled ocean crust and sediment in Indian Ocean MORB. *Earth Planet. Sci. Lett.* **147**, 93–106.

Roeder, P. and Emslie, R. F. (1970) Olivine-liquid equilibrium. *Contrib. Mineral. Petrol.* **29**, 275–280.

Sarda, P., Moreira, M., Staudacher, T., Schilling, J-G. and Allegre, C. J. (2000) Rare gas systematics on the southernmost Mid-Atlantic Ridge: constraints on the lower mantle and the Dupal source. *J. Geophys. Res.* **105**, 5973–5996.

Schiano, P. (2003) Primitive mantle magmas recorded as silicate melt inclusions in igneous minerals. *Earth-Science Reviews* **63**, 121–144.

Scowen, P. A. H., Roeder, P. L. and Helz, R. T. (1991) Reequilibration of chromite within Kilauea Iki lava lake, Hawai. *Contrib. Mineral. Petrol.* **107**, 8–20.

Sims, K. W. W., Goldstein, S. J., Blichert-Toft, J., Perfit, M. R., Kelemen, P., Fornari, P., Michael, P., Myrrel, M. T., Hart, S. R., De Paolo, D. J., Layne, G., Ball, L., Jull, M. and Bender, J. (2002) Chemical and isotopic constraints on the generation of magma beneath the East Pacific Rise. *Geochim. Cosmochim. Acta* **66**(19), 3481–3504.

Sinton, C. W., Christie, D. M., Coombs, V. L., Nielsen, R. L. and Fisk, M. R. (1993) Near primary melt inclusions in anorthite phenocrysts from the Galapagos platform. *Earth Planet. Sci. Lett.* **119**, 527–537.

Slater, L. D., Mckenzie, K., Gronvold, K. and Shimizu, N. (2001) Melt generation and movement beneath Theistareykir, NE Iceland. *J. Petrol.* **42**, 321–354.

Sobolev, A. V. and Shimizu. N. (1993) Ultradepleted primary melt included in an olivine from the Mid Atlantic Ridge. *Nature* **363**, 151–154.

Sobolev, A. V., Hofmann, A. W. and Nikogosian, I. K. (2000) Recycled oceanic crust observed in 'ghost plagioclase' within the source of Mauna Loa lavas. *Nature* **404**, 986–989.

Sours-Page, R., Johnson, K. T. M., Nielsen, R. L. and Karsten, J. L. (1999) Local and regional variation of MORB parent magmas: evidence from melt inclusions from the Endeavour Segment of the Juan de Fuca Ridge. *Contrib. Mineral. Petrol.* **134**, 342–363.

Sun, S. S. and McDonough, W. F. (1989) Chemical and isotopic systematics of oceanic basalts: implications for mantle composition and processes. Magmatism in the Ocean Basins. *Geological Society Special Publication* **42**, 313–345.

Tronnes, R. G. (1990) Basaltic melt evolution of the Hengill volcanic system, SW Iceland, and evidence for clinopyroxene assimilation in primitive tholeiitic magmas. *J. Geophys. Res.* **95**, 15893–15910.

Unrug, R. (1996) The assembly of Gondwanaland. *Episodes* **19**, 11–20.